Mon. Not. R. Astron. Soc. 000, 1–15 (2003) Printed 11 March 2003 (MN LATEX style file v2.2)

SUMSS: A Wide-Field Radio Imaging Survey of the Southern Sky. II. The Source Catalogue

T. Mauch,[1⋆] T. Murphy,[1†] H.J. Buttery,[2] J. Curran,[3‡] R.W. Hunstead,[1]
B. Piestrzynski,[1] J.G. Robertson,[1] E.M. Sadler[1]
[1] School of Physics, University of Sydney, NSW, 2006, Australia.
[2] Cavendish Laboratory, University of Cambridge, Cambridge CB3 OHE, UK.
[3] School of Information Technologies, University of Sydney, NSW, 2006, Australia.

Accepted 2003 March 7.

ABSTRACT

This paper is the second in a series describing the Sydney University Molonglo Sky Survey (SUMSS) being carried out at 843 MHz with the Molonglo Observatory Synthesis Telescope (MOST). The survey will consist of ~ 590 $4.3^\circ \times 4.3^\circ$ mosaic images with $45'' \times 45''\mathrm{cosec}|\delta|$ resolution, and a source catalogue. In this paper we describe the initial release (version 1.0) of the source catalogue consisting of 107,765 radio sources made by fitting elliptical gaussians in 271 SUMSS $4.3^\circ \times 4.3^\circ$ mosaics to a limiting peak brightness of 6 mJy beam^{-1} at $\delta \leq -50^\circ$ and 10 mJy beam^{-1} at $\delta > -50^\circ$. The catalogue covers approximately 3500 deg^2 of the southern sky with $\delta \leq -30^\circ$, about 43 per cent of the total survey area. Positions in the catalogue are accurate to within $1'' - 2''$ for sources with peak brightness $A_{843} \geq 20$ mJy beam^{-1} and are always better than $10''$. The internal flux density scale is accurate to within 3 per cent. Image artefacts have been classified using a decision tree, which correctly identifies and rejects spurious sources in over 96 per cent of cases. Analysis of the catalogue shows that it is highly uniform and is complete to 8 mJy at $\delta \leq -50^\circ$ and 18 mJy at $\delta > -50^\circ$. In this release of the catalogue about 7000 sources are found in the overlap region with the NRAO VLA Sky Survey (NVSS) at 1.4 GHz. We calculate a median spectral index of $\alpha = -0.83$ between 1.4 GHz and 843 MHz. This version of the catalogue will be released via the World Wide Web with future updates as new mosaics are released.

Key words: catalogues – surveys – methods: data analysis – astrometry – galaxies: statistics – radio continuum: general

1 INTRODUCTION

Paper I of this series (Bock et al. 1999) described the survey design and science goals of the Sydney University Molonglo Sky Survey (SUMSS). SUMSS is imaging the southern ($\delta < -30^\circ$) radio sky at 843 MHz with similar sensitivity and resolution to the northern NRAO VLA Sky Survey (NVSS; Condon et al. 1998) at 1.4 GHz.

SUMSS uses the Molonglo Observatory Synthesis Telescope (MOST; Mills 1981; Robertson 1991), a 1.6 km-long cylindrical paraboloid reflector which has the largest collecting area of any telescope in the southern hemisphere. The MOST was upgraded in 1996–97 to give it a 2.7° diameter field of view (Large et al. 1994; Bock et al. 1999), and since mid-1997 over 90 per cent of MOST observing time has been devoted to SUMSS. The survey will be completed by the end of 2003.

In this paper, we present the first part of the SUMSS source catalogue, covering 3500 deg^2 of the southern sky. The catalogue will be updated regularly as the survey progresses, and a version is available online at www.astrop.physics.usyd.edu.au/sumsscat/.

The structure of the paper is as follows. In Section 2 we describe the software used to construct the catalogue and the procedures to construct the source list. In Section 3 we describe our technique for removing spurious responses from the catalogue. In Section 4 we describe the uncertainties in

⋆ E-mail: tmauch@physics.usyd.edu.au
† Present address: Institute of Astronomy, University of Edinburgh, Royal Observatory, Blackford Hill, Edinburgh EH9 3HJ, UK.
‡ Present address: Institute for Communicating and Collaborative Systems, School of Informatics, University of Edinburgh, 2 Buccleuch Place, Edinburgh, EH8 9LW, UK.

the catalogue. Finally, Section 5 contains our analysis of the catalogue.

2 CATALOGUE CONSTRUCTION

The individual 2.7° diameter fields of the survey were combined to form 4.3° × 4.3° mosaics. The field centres are located on a grid of overlapping pointing centres such that, when combined, sensitivity is recovered in the overlap regions making the noise in the resulting mosaics almost uniform (Bock et al. 1999). The mosaic centres are located on a grid which matches that for the NVSS mosaics, but is extended to the south celestial pole. This initial release of the SUMSS catalogue was built on 2002 February 25 using 271 of the ∼ 590 mosaics in the complete survey. Figure 1 shows the positions of all 107,765 sources currently in the catalogue and gives a representation of the sky coverage of this release.

Extracting sources from astronomical images is a well documented problem and there are currently many computer programs which will find and characterise sources in images such as those in SUMSS. We decided to use the AIPS task VSAD, written for the NVSS survey (Condon et al. 1998), which locates sources in an image and fits elliptical gaussians to them. This was to ensure uniformity between SUMSS and NVSS, and also because our tests showed that VSAD fitted sources more reliably than other programs such as IMSAD in the MIRIAD package (Sault et al. 1995).

Most of the sources in the SUMSS survey are well fitted by an elliptical gaussian model because the majority of extragalactic radio sources are smaller than the MOST restoring beam of $45'' \times 45''\mathrm{cosec}|\delta|$ (Windhorst et al. 1990). The current release of the SUMSS catalogue does not cover the Molonglo Galactic Plane Survey (MGPS-2; Green 1999) region ($|b| < 10°$) because complex source structures in the Galactic plane make elliptical gaussian fits unsatisfactory. However, there is little contamination by complex Galactic sources in MGPS-2 mosaics as close to the Galactic plane as $|b| = 2°$, so in the future it will be possible to visually inspect regions closer to the Galactic plane to decide those which can be included in the catalogue using current methods. In extremely complex regions we intend to cross-match the MGPS-2 mosaics with source catalogues at other frequencies (eg. IRAS PSC; Beichman et al. 1988 & RASS; Voges 1992).

2.1 Source Fitting

VSAD was used to find radio sources in each of the 4.3° × 4.3° mosaics in the SUMSS survey and fit an elliptical gaussian to them. The parameters of each gaussian returned by VSAD are the J2000 right ascension α and declination δ (both in degrees), peak brightness A_{843} (mJy beam^{-1}), total flux density S_{843} (mJy), FWHM fitted source major and minor axes $\theta_{\mathrm{M}}, \theta_{\mathrm{m}}$ (arcseconds) and the fitted position angle of the major axis (degrees east from north). VSAD also creates a residual image by subtracting each fitted gaussian from the input image.

Figure 2 shows a small region of an illustrative SUMSS mosaic (J0000M84[1]) overlaid with the gaussians fitted by VSAD. Most sources on the original mosaic are well fitted by gaussians, though some artefacts close to stronger sources are also fitted. It can be seen from the complex structure in Figure 2 that VSAD can be unreliable for close pairs of sources in extreme cases. Occasionally two distinct sources are fitted incorrectly as a single gaussian with major axis greater than the true separation of the sources (eg. the 38.6 mJy extended source in Figure 2.). Almost all close doubles remain in the final version of the catalogue as separate sources.

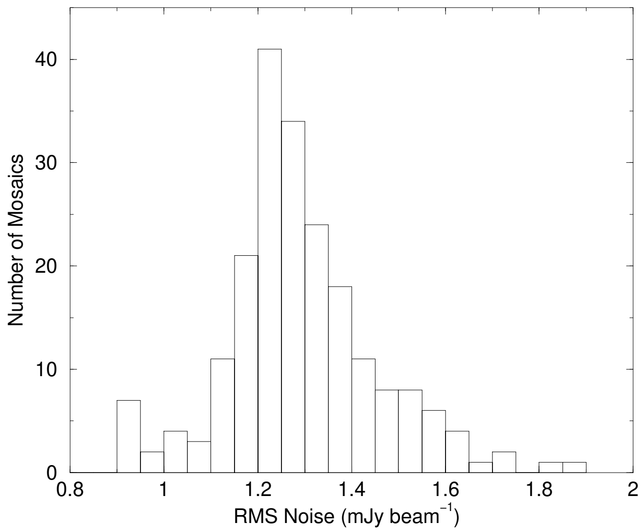

Figure 3. A histogram of the rms noise measured in the mosaics at $\delta \leq -50°$. Most of the mosaics have rms values ∼ 1.2 − 1.3 mJy beam^{-1}; the mode is 1.25 mJy beam^{-1}. The tail at higher rms values is due to mosaics containing bright sources which tend to increase the local rms noise.

2.2 Noise

Even though the field tiling patterns were designed to make the resulting noise in the mosaics uniform, background noise is higher in localised regions close to strong sources. We determined the rms noise in the SUMSS survey to establish a threshold below which sources are discarded from the catalogue. The residual images created by VSAD were kept and used to estimate the local rms noise for each source. Two estimates of the rms noise were obtained:

(i) First the noise was estimated over each residual image by fitting a normal curve to the pixel distribution giving an estimate of the average noise over the area of each entire mosaic. Figure 3 shows the distribution of rms values obtained in this way. The median rms noise of the mosaics at $\delta \leq -50°$ is 1.27 mJy beam^{-1}. For $\delta > -50°$ the scatter is much greater as the rms noise increases strongly with declination north of −50° (see Figure 4). The median value of rms noise at $\delta > -50°$ is 1.9 mJy beam^{-1}. Hereafter we refer

[1] The naming scheme for SUMSS mosaics is J*hhmm*M*dd* where J signifies J2000 coordinates, *hhmm* is the RA in hours and minutes of the mosaic centre, M signifies southern declination and *dd* is the declination of the mosaic centre in degrees.

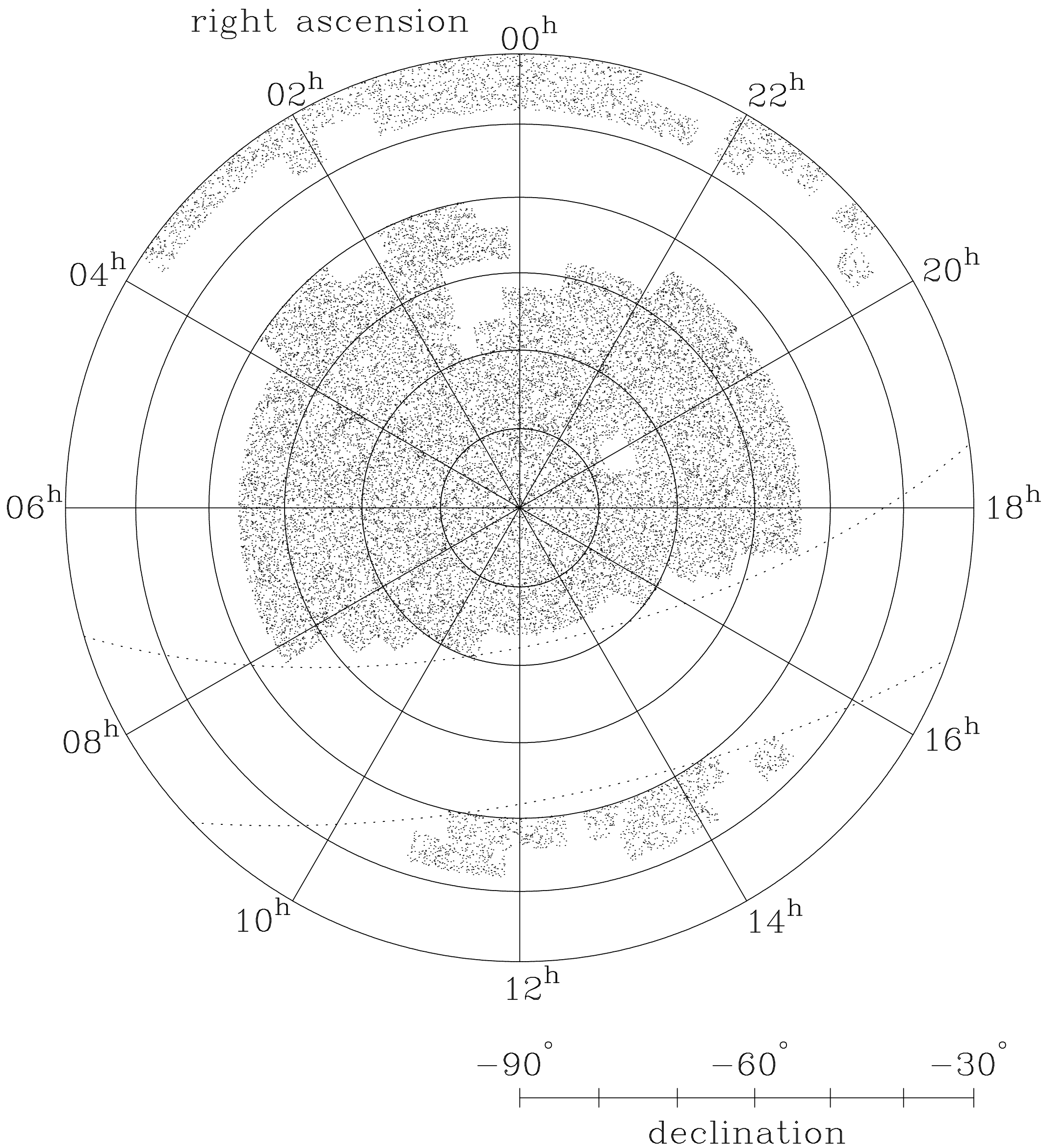

Figure 1. A plot in the equal-area Lambert projection of all 107,765 sources in the 271 mosaics in version 1.0 of the SUMSS catalogue. The total sky coverage is 3500 deg^2. Dotted lines are drawn at $b = \pm 10°$ to indicate the location of the Galactic plane. The source density is lower at declinations north of $-50°$ due to the higher flux density limit ($S_{843\mathrm{MHz}} \geq 10$ mJy). There is a significant underdensity of sources around $\delta = -45°, \alpha = 13h$; this is because of the large number of artefacts in the vicinity of Centaurus A, which obscure weak sources.

to regions at $\delta \leq -50°$ as southern and those $\delta > -50°$ as northern.

(ii) Secondly, a local rms for each source was determined by computing a pixel histogram in a box of 100×100 pixels (∼600 beams) in the residual image and fitting a normal curve to this distribution. The distribution was clipped so as to only include pixels within ± 5 times the rms noise measured in the mosaics. Residual artefacts from strong sources tend to increase the estimate of local rms noise. By this method we have an estimate of the local rms noise for each source which takes into account increases in the noise level close to bright sources. Values of local rms noise close to bright sources are 3–4 times greater than those in other regions, because of the limited dynamic range ($\sim 100:1$) of the MOST (Bock et al. 1999).

Figure 4 shows the variation in local rms noise with declination for stronger sources ($S_{843} > 50$ mJy) in the present survey release. The gain of the MOST varies with Meridian Distance[2] (MD) due to a number of factors arising from the structure of the telescope. For example the cosec$|\delta|$-shaped rise towards northern declinations is due to the foreshortening of the MOST at large |MD|. A model of the rms noise variation with declination is plotted. This was determined by summing the noise variance as a function of hour angle, taking into account the variation of noise due to the MOST

[2] The Meridian Distance (MD) at declination δ and hour angle H is given by $\sin(\mathrm{MD}) = \cos\delta \sin H$. This is explained in more detail in Paper I (Bock et al. 1999).

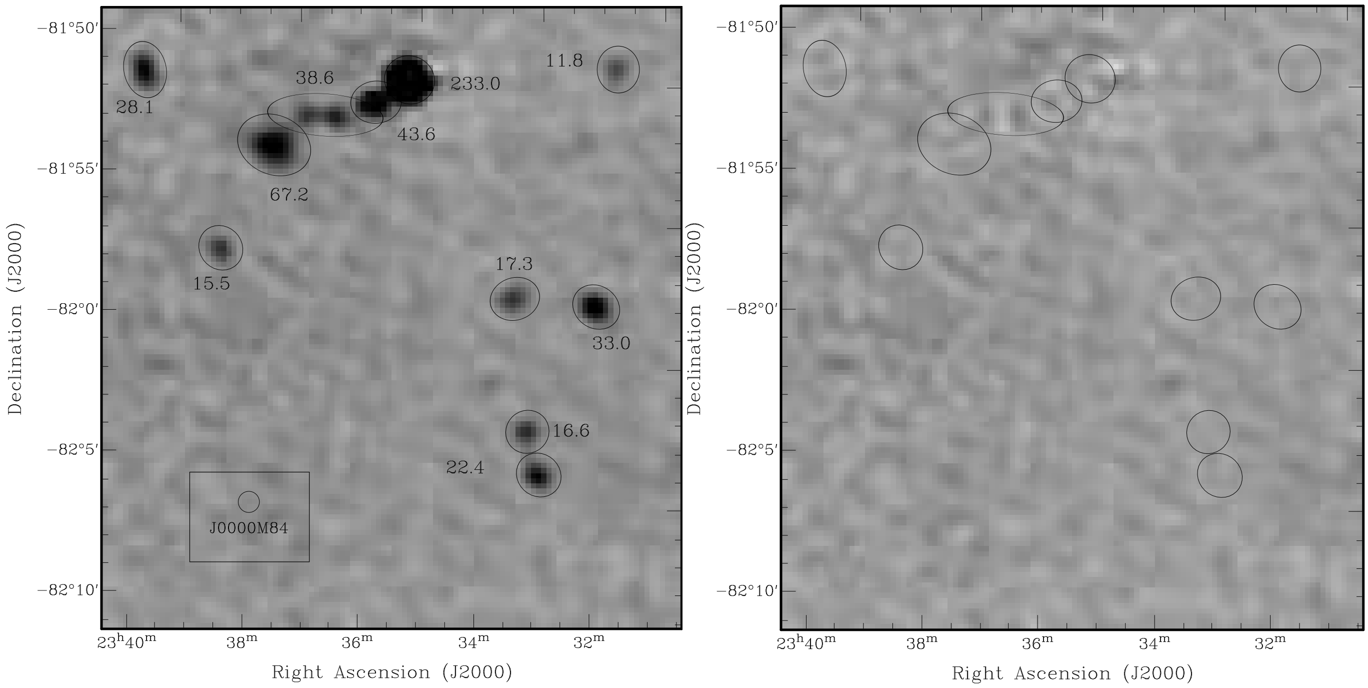

Figure 2. Left: A small section of the mosaic J0000M84 with ellipses fitted by VSAD. The total flux density (in mJy) of each source is printed beside it. The beam is shown as a small circle on the bottom left of the image. One close double is fitted as a single gaussian, while another is fitted as two. Right: The residual image of the same region after subtraction of the fitted gaussians. The improperly fitted source in the north has resulted in residual flux in this image.

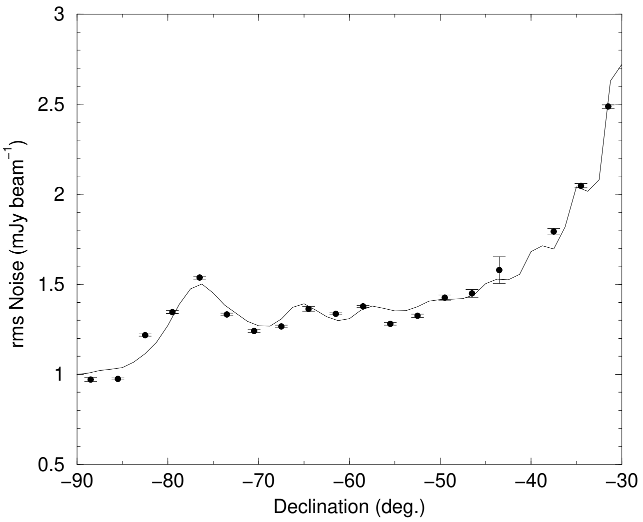

Figure 4. A plot of median rms noise computed around brighter sources ($S_{843} > 50$ mJy) vs. declination. The line drawn is a model based on the MOST MD gain curve. It is shown to indicate the effect of the variation of the MOST gain with declination. The noise peak at $\delta = -76°$ is explained by this curve. The rms noise increases sharply north of $\delta \sim -50°$, which is the declination above which we increase the brightness limit of the catalogue to 10 mJy beam^{-1} .

MD gain curve. This curve matches the observed rms noise variation quite well.

VSAD was used to fit all peaks brighter than 5 mJy beam^{-1} at $\delta \leq -50°$ and 10 mJy beam^{-1} at $\delta > -50°$. Typically about 400 gaussians were fitted in the northern mosaics and about 700 in the southern ones. VSAD fitted many noise peaks and artefacts in the southern mosaics between 5 and 6 mJy beam^{-1}. We decided to set the catalogue limit at 6 mJy beam^{-1} at $\delta \leq -50°$ and 10 mJy beam^{-1} at $\delta > -50°$.

2.3 Duplicate Sources

The VSAD routine was run separately on each mosaic resulting in a total list of 171,846 responses over the 3500 deg^2 of survey area currently complete. This list was then pruned to remove multiple entries and spurious sources arising from image artefacts. The SUMSS survey was designed such that the mosaics created from the individual observations overlapped slightly (Bock et al. 1999). This overlap changes with declination from about 50 per cent at $\delta = -88°$ to 1–2 per cent at $\delta = -32°$. Therefore some entries in the total list are multiple occurrences of sources which have appeared in overlapping mosaics.

Figure 5 is a plot of the distribution of source separations for a subset of about 40,000 sources in the raw catalogue. The distribution has a minimum at 45″ after which the contribution of genuine close doubles causes it to rise again. This minimum is not surprising given that the beamwidth of the survey is $\sim 45''$. Sources appearing in different mosaics with position differences less than 45″ were flagged as possible duplicates.

Once a group of duplicate sources has been identified the following criteria are used to select which source to retain from that group:

(i) If there are more than two sources then the peak amplitudes of all the sources are compared and those with peak

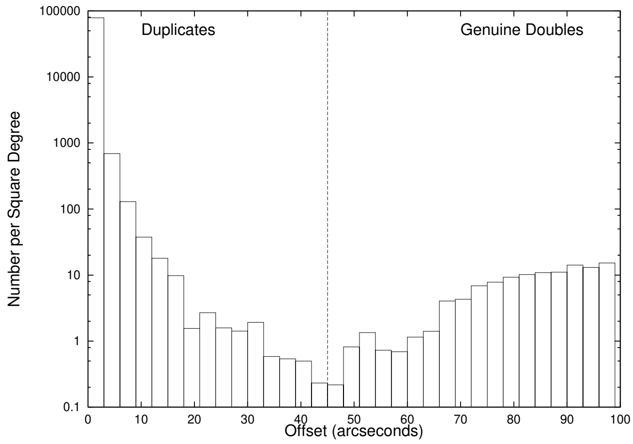

Figure 5. The distribution of source separations for the raw version of the SUMSS catalogue. The number of sources found at different radii has been divided by the sky area to obtain the source density versus separation. The minimum at about 45″ is taken as the separation beyond which the number of close doubles dominates over the number of duplicates. There is a small number of sources with separations between 45″ and 75″; these are the result of overlapping gaussians fitted by VSAD. Above 80″ the distribution flattens as expected.

amplitude greater than twice or less than half the average are ignored. This can occur when some artefacts are fitted at the position of another source.

(ii) Sources closer than 10 pixels from the edge of a mosaic are ignored to ensure that extended sources are not fitted over the edge of the image. If all sources are further than 10 pixels from the edge then option (iii) is used.

(iii) If there is still more than one source to select, the source with the lowest local rms noise has its fitted parameters recorded in the catalogue.

These criteria ensure that one source is selected out of a set of multiple detections. Generally only two sources need to be compared and the one with the lower local rms noise is placed in the catalogue. A flag telling how many other mosaics the selected source appears in is included in the final catalogue. The source which is listed in the catalogue can be considered the best-fitting source from VSAD. In compiling the current version of the catalogue, about 45,000 sources were removed because they appear more than once in the raw catalogue.

3 IMAGE ARTEFACTS

The images in SUMSS are affected by a number of artefacts, many of which are fitted by the VSAD routine as sources. Classification of artefacts is a difficult problem, as they vary enough in shape and strength that no simple method can be used to separate them from real sources. The images in Figure 6 show the variety of artefacts in SUMSS images and some examples of elliptical gaussians which VSAD has fitted to them. About 10 per cent of sources in the raw SUMSS catalogue are fits to artefacts.

Table 1. Confusion matrices comparing decision tree classification with hand classification. Left: Results of southern decision tree on test data. Right: Results of northern decision tree on test data.

Southern

Class (hand)	(decision tree) (1)	(2)	(3)
(1)	12		5
(2)	1	2	
(3)	1	3	618

Northern

Class (hand)	(decision tree) (1)	(2)	(3)
(1)	3	1	1
(2)	2	1	
(3)	3		415

3.1 Types of Artefacts

There are two common artefacts which are fitted as genuine sources by VSAD, *grating rings* and *radial spokes*.

Grating rings arise from the periodic structure of the MOST array. They appear as ellipses of semi-diameter $n(1.15° \times 1.15°\mathrm{cosec}|\delta|)$ where n is an integer denoting the order of the grating ring. Grating rings increase in strength up to the fourth order ring. While grating rings are not uniquely a problem of the MOST, it is not possible to remove them using the standard CLEAN routine. This is because the effective primary beam of the MOST varies with time and is not azimuthally symmetric. Also individual baseline visibilities are not recorded during MOST observations (Mills 1981; Robertson 1991). It is possible that in future an improved CLEAN routine might be written to remove grating rings by accurately modelling the MOST primary beam. The future upgrade of the telescope as an SKA demonstrator (SKAMP; Green et al. 2001) will eliminate this problem, as all the baseline visibilities will be retained with each observation and application of self calibration algorithms will be possible. The amplitude of grating rings is also dependent on the position of the source in the original SUMSS field so the mosaicing process can cause abrupt steps in their strength. This effect can be seen in the leftmost image of Figure 6, where a strong fourth-order grating ring associated with a 5.4 Jy source abruptly becomes weaker.

Radial spokes appear as long thin bands stretching away radially from a source. They are believed to be caused by random shifts of order 1″ in the position of the comb of MOST fan beams, on a time-scale of minutes (Bock et al. 1999). The shifts are believed to occur due to weather related anomalies in the local oscillator phase or irregularities in ionospheric or tropospheric refraction. Some radial spokes are shown in the middle image of Figure 6 and almost always appear as highly elongated sources in the output of VSAD. Generally such artefacts are only fitted close to sources with peak brightness greater than 500 mJy beam^{-1}, because the peak amplitude of radial spokes then becomes stronger than 6 mJy beam^{-1}. The source density close to extremely bright sources in SUMSS can decrease substantially as radial spokes can raise the local rms noise level by up to 3-4 times.

3.2 Response Classification with a Decision Tree

The variety and complexity of artefacts fitted as sources make it difficult to classify sources as genuine or spurious in a simple way. We have employed the *decision tree* program

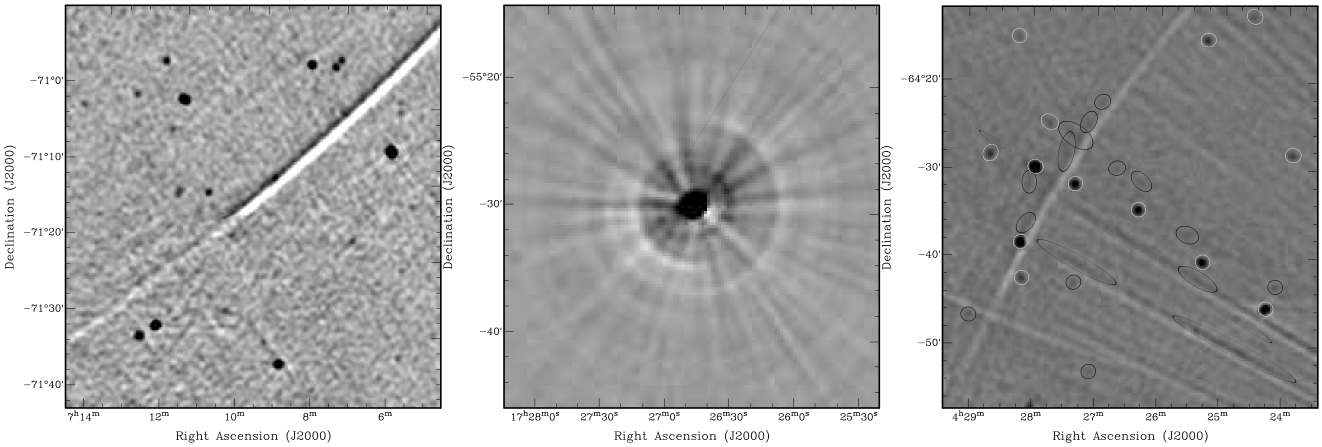

Figure 6. Three images showing the variety of artefacts present in SUMSS mosaics which are fitted as spurious sources by VSAD. The left image shows part of a grating ring associated with a 5.46 Jy source (PKS B0743–673) at RA = $07^{\rm h}\,43^{\rm m}\,32\overset{\rm s}{.}67$, Dec. = $-67^\circ\,26'\,28\overset{''}{.}4$ (J2000). Its sudden weakening occurs because the ring appears in different parts of two 2.7° fields which make up the mosaic. The middle image shows a 1.8 Jy source and the radial spikes associated with it. The spikes here have peak amplitude of 10 mJy beam^{-1} and extend about 30′ away from the source. The right image shows a small area of the SUMSS mosaic J2100M72 with many artefacts. Radial spokes of average peak amplitude $\sim$ 6 mJy beam^{-1} are visible, as is a weak grating ring. Ellipses fitted by VSAD are overlaid on the image. Sources classified by the decision tree as artefacts are shown as black ellipses and sources classified as genuine are shown as white ellipses.

C4.5 (Quinlan 1993) to aid in the classification of sources in the mosaics. A decision tree encodes a classification function as a hierarchy of tests which classify examples into different classes. Each example consists of a set of attributes, each with an associated value.

The tree represents the classification function as follows:

(i) Every internal node corresponds to a test examining one or more attributes of the example to be classified.
(ii) Each branch descending from the node corresponds to a particular outcome of the test.
(iii) Finally, the leaf nodes in the tree are labelled with the class to assign.

C4.5 is a popular, freely available decision tree learner. Another application of a decision tree to radio source catalogues can be found in the FIRST survey (White et al. 1997).

The raw output from VSAD includes about 39 source characteristics which can be used as attributes for the decision tree; these include the fitted and deconvolved source sizes and the raw fitting uncertainties quoted by VSAD. We have also included some extra parameters mainly relating each fitted source to the nearest strong source, including separation and relative position angle. Because of the different properties of the MOST beam in the two regions, we made two separate decision trees, one for the southern catalogue $\delta \leq -50^\circ$ and one for the northern catalogue $\delta > -50^\circ$.

The decision tree program was trained by hand on a subset of mosaics with many artefacts. About 3000 sources in the south and about 1500 sources in the north were hand classified. To ensure that the training was reliable, each source was examined separately by at least two of us, and the final decision on each source was made by one of us (Mauch) comparing the two human classifications, thereby minimising the subjective judgement of each human classifier. About 10 per cent of human classifications were changed during comparison. The objects contained in the raw output of VSAD were classified using a numbering scheme from 1-3 with the following definitions.

(1) The source is an artefact.
(2) The source is in a region of low signal-to-noise.
(3) The source is real.

The decision tree was then run and the result for both the northern and southern decision trees was tested on a small independent sample of hand classified sources from one mosaic. Table 1 shows the results from this test. It can be seen from analysis of the training data that artefacts tend to be correctly identified. In some cases a hand classified type 1 source is machine classified as type 2 and vice versa but it is rare for sources hand classified as 1 or 2 to be machine classified as genuine. Conversely only a small number of type 3 sources have been classified as artefacts. This does have an effect on the completeness of the survey at flux densities of 6–10 mJy (Figures 11 & 15 in Section 6 show this more clearly). Overall the accuracy of the decision tree on the testing data is conservatively estimated to be 96 per cent. The accuracy for the entire catalogue is probably a little lower, but most of the misclassified sources are real sources which were classified as artefacts. This implies that the final version of the catalogue should be very reliable.

The decision tree was found to be least reliable for extended sources with major axis length greater than five times their minor axis length. Every such source classified as genuine by the decision tree was double checked by hand. About 10 per cent of these classifications were found to be incorrect.

The final released catalogue only contains sources classified as genuine by the decision tree. The unmodified catalogue contains 10 per cent extra sources, most of which are artefacts. This larger (but less reliable) catalogue with an extra column containing decision tree classifications, will be available on request.

4 ACCURACY

All of the uncertainties calculated in the catalogue are a combination of both fitting and calibration uncertainties of the MOST. In general the calibration uncertainties of the MOST are small and the fitting uncertainties tend to dominate. Fitting uncertainties for the SUMSS catalogue were determined using equations derived in Condon (1997) (herafter C97). The noise in SUMSS mosaics is correlated at the length scale of the restoring beam of MOST. As this beam is elliptical, the axis length of the restoring beam was taken as the noise correlation length in SUMSS ($\theta_{\rm N}^2 = b_{\rm M} b_{\rm m} = 45'' {\rm cosec}|\delta| \times 45''$; where $b_{\rm M}, b_{\rm m}$ are widths of the MOST beam major and minor axes respectively). This implies that the effective signal-to-noise ratio (ρ) is given by:

$$\rho^2 = \frac{\theta_{\rm M}\theta_{\rm m}}{4\theta_{\rm N}^2}\left[1+\left(\frac{\theta_{\rm N}}{\theta_{\rm M}}\right)^2\right]^{\alpha_{\rm M}}\left[1+\left(\frac{\theta_{\rm N}}{\theta_{\rm m}}\right)^2\right]^{\alpha_{\rm m}}\frac{A_{843}^2}{\sigma^2}, \quad (1)$$

where $\theta_{\rm M}$ is the fitted major axis size and $\theta_{\rm m}$ is the fitted minor axis size. A_{843} is the peak brightness of the fitted Gaussian and σ is the rms noise of each mosaic (C97); σ is taken to be the local rms noise as derived in Section 2.1. For the uncertainties in each fitted parameter we have used the same empirical values for the exponents $\alpha_{\rm M}$ and $\alpha_{\rm m}$ taken from C97 and also used in the NVSS source catalogue (Condon et al. 1998).

4.1 Position Uncertainties

The fitting variances in the source positions are given by:

$$\sigma_\alpha^2 = \sigma_{\rm M}^2 \sin^2({\rm PA_F}) + \sigma_{\rm m}^2 \cos^2({\rm PA_F}), \quad (2)$$

$$\sigma_\delta^2 = \sigma_{\rm M}^2 \cos^2({\rm PA_F}) + \sigma_{\rm m}^2 \sin^2({\rm PA_F}), \quad (3)$$

where the rms noiselike uncertainties of the fitted major and minor axes $\sigma_{\rm M}$ and $\sigma_{\rm m}$ are derived as in equation 25 of C97. $\rm PA_F$ is the fitted position angle of the source in degrees east of north. The fitting uncertainties become quite large ($\sim 5''$) for weaker extended sources ($A_{843} < 10\,{\rm mJy\,beam^{-1}}$).

For sources with $S_{843} \geq 50\,$mJy the calibration uncertainty of the MOST is greater than the fitting uncertainties. We have determined the calibration uncertainty for stronger sources ($S_{843} > 200\,$mJy) by comparison with positions in the NVSS catalogue in the overlap region between SUMSS and NVSS ($-40^\circ < \delta < -30^\circ$; $464\,{\rm deg}^2$ in the current release). The positions of strong sources in the NVSS catalogue are known to be accurate to within $(\epsilon_\alpha, \epsilon_\delta)$=(0$''$.45, 0$''$.56) (Condon et al. 1998). Only point sources in SUMSS were used in this comparison to avoid the larger position uncertainties associated with extended sources. There are about 500 SUMSS sources which meet these criteria in the overlap region, all of which have a counterpart in the NVSS catalogue. Figure 7 contains a plot of the offsets in Right Ascension ($\Delta\alpha$) and Declination ($\Delta\delta$) between NVSS and SUMSS. The mean offsets are $\langle\Delta\alpha\rangle = -0''.59 \pm 0''.07$ and $\langle\Delta\delta\rangle = -0''.30 \pm 0''.08$. These offsets are caused by a combination of both calibration errors in individual fields and fitting errors. No correction has been applied to the final version of the catalogue. For more information about SUMSS position uncertainties, see Paper I (Bock et al. 1999).

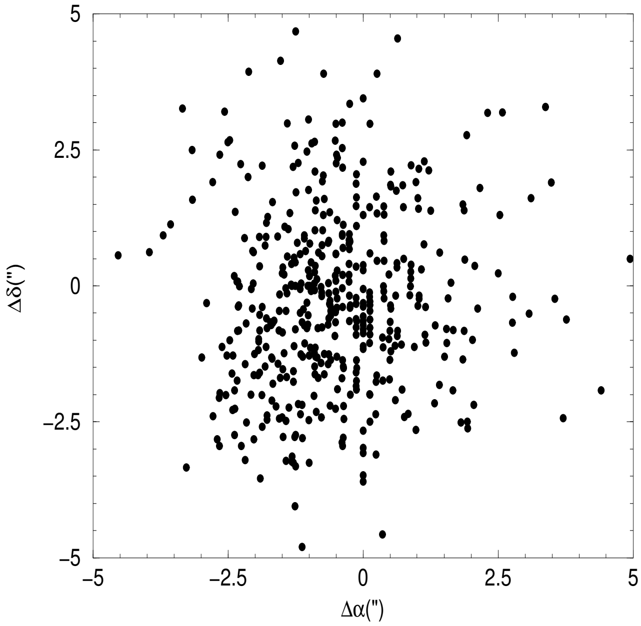

Figure 7. A plot of the offset (SUMSS position minus NVSS position) in both Right Ascension (α) and Declination (δ) between 500 bright point sources in the overlap region between SUMSS and NVSS.

The rms of the offsets between the SUMSS and NVSS catalogues have been used to determine the SUMSS position calibration uncertainties. These are $\epsilon_\alpha = 1''.5$ for Right Ascension and $\epsilon_\delta = 1''.7$ for Declination. The elongation of the MOST beam at $\delta \geq -40^\circ$ means the rms in declination is larger than in the southern catalogue, implying that these values are a conservative estimate of the MOST position uncertainty in declination. The calibration uncertainties quoted here have been added in quadrature to the fitting uncertainties for each source to obtain the position uncertainties in the catalogue.

4.2 Source Sizes

The uncertainties in the axes of the elliptical gaussians fitted by VSAD ($\sigma(\theta_{\rm M}), \sigma(\theta_{\rm m})$) are determined by combining in quadrature equation 21 of C97 and the calibration uncertainty in the major and minor axes of the MOST beam shape. The MOST beam calibration uncertainty has been determined by examining fits to moderately strong sources believed to be unresolved. Because fits to the strongest sources with $S_{843} > 500\,$mJy could be contaminated by image artefacts, only moderately strong ($100\,{\rm mJy} < S_{843} < 500\,{\rm mJy}$) sources were chosen. From this analysis we have conservatively estimated the beam calibration uncertainty to be $\epsilon_\theta = 3$ per cent in both axes. The uncertainty is worst in the northern mosaics in which the beam is considerably elongated. The probability that the fitted size of a point source would be larger than the beam by more than $2.33\sigma(\theta_{\rm M,m})$ is 2 per cent so we compare the beam plus $2.33\sigma(\theta_{\rm M,m})$ with the major and minor fitted axis lengths to determine if a source is resolved along either axis.

Sources for which either the major axis or both fitted axes are believed to be resolved are then deconvolved along each resolved axis. The fitted gaussians in the raw output of

VSAD are the convolution of the MOST elliptical beam with the true source shape. The deconvolved major and minor axis widths of each fitted source ($\phi_{\rm M}, \phi_{\rm m}$) were found using

$$2\phi_{\rm M}^2 = (\theta_{\rm M}^2 + \theta_{\rm m}^2) - (b_{\rm M}^2 + b_{\rm m}^2) + \beta, \quad (4)$$

$$2\phi_{\rm m}^2 = (\theta_{\rm M}^2 + \theta_{\rm m}^2) - (b_{\rm M}^2 + b_{\rm m}^2) - \beta, \quad (5)$$

where $\theta_{\rm M}, \theta_{\rm m}$ are the fitted major & minor axes of the source, $b_{\rm M}, b_{\rm m}$ are the beam major & minor axes and β is given by

$$\beta^2 = (\theta_{\rm M}^2 - \theta_{\rm m}^2)^2 + (b_{\rm M}^2 - b_{\rm m}^2)^2 - 2(\theta_{\rm M}^2 - \theta_{\rm m}^2)(b_{\rm M}^2 - b_{\rm m}^2)\cos 2\,({\rm PA_F} - {\rm PA_B})\,, \quad (6)$$

where $\rm PA_F$ and $\rm PA_B$ are the position angles of the fitted source and the MOST beam (Wild 1970). The MOST beam is oriented north-south so $\rm PA_B = 0$ always.

The ellipticity of the MOST beam causes the fitted position angle to differ from the true source position angle ($\rm PA_S$). We find the deconvolved major axis position angle using

$$\tan(2{\rm PA_S}) = \left[\frac{(\theta_{\rm M}^2 - \theta_{\rm m}^2)\sin 2{\rm PA_F}}{(\theta_{\rm M}^2 - \theta_{\rm m}^2)\cos 2{\rm PA_F} - (b_{\rm M}^2 - b_{\rm m}^2)}\right]. \quad (7)$$

A deconvolved source size is quoted for each resolved source in the catalogue. No source sizes are given for unresolved sources. It should be noted that the fitted source sizes and deconvolved source sizes in the catalogue are only intended to be indicative of the true source structure. Sometimes more extended sources are the result of a poor fit by the VSAD program (see Figure 2) and the original images are the best guide in determining whether or not a given radio source is resolved.

4.3 Flux Density

The uncertainties in the fitted peak brightness in SUMSS images are calculated as the quadratic sum of the MOST internal flux density calibration uncertainty and the local noise uncertainty. The local noise uncertainty is calculated using

$$\sigma_{A_{843}}^2 = \frac{A_{843}^2}{\rho^2}, \quad (8)$$

where $\alpha_M = \alpha_m = 3/2$ was used in the calculation of ρ^2 from Equation 1 (Condon et al. 1998).

To calculate the flux density calibration uncertainty of the MOST we used results from a detailed analysis of the Molonglo calibrators (Gaensler & Hunstead 2000). Before and after every 12-hour observation the MOST measures the flux densities of ∼5 compact sources, chosen from a list of 55 calibrators. Observations of the calibrators in the period 1984 to 1996 have been extracted from the MOST archive and used to determine the calibration uncertainty of the MOST. Gaensler & Hunstead (2000) examined the variability of the calibrators in this period and found that 19 of these showed no variability in this time. We have chosen 7 of the non-variable calibrators with flux densities > 5 Jy which were observed at a meridian distance $|{\rm MD}| < 30°$ to ensure that errors resulting from fan-beam confusion and uncertainty in the meridian distance gain curve at higher MD were minimised. Table 2 shows the results of this analysis.

The average scatter in flux density measurements $\epsilon_{A_{843}}$ is around 3 per cent. We have adopted this value as the internal calibration uncertainty of MOST peak brightness measurements. Peak brightness uncertainties in the catalogue are obtained by adding $\epsilon_{A_{843}} A_{843}$ and $\sigma_{A_{843}}$ in quadrature.

The integrated flux density of each source is calculated from the parameters of the gaussian fit and depends on whether or not the source is significantly resolved. We use the same equations to derive the total flux density as those described for NVSS (Condon et al. 1998). The fitting uncertainties in integrated flux density are the same as those quoted in C97.

The quoted flux density uncertainties do not take account of the errors which arise from fitting an extended gaussian to a source with complex structure. Extended sources are often fitted poorly by an elliptical gaussian model and this can lead to unreliable estimates of the true integrated flux density. Users should therefore note that for some extended sources the quoted flux density and source sizes will be incorrect by more than the quoted uncertainties.

The flux density scale at 843 MHz was determined partly by absolute measurements and partly by interpolation between measurements at 408 MHz (Molonglo) and 2700 MHz (Parkes) (Hunstead 1991). To check the accuracy of the total flux densities quoted in the SUMSS catalogue we have examined the distribution of spectral indices between the SUMSS catalogue at 843 MHz and the NVSS catalogue at 1.4 GHz. Flux densities in the NVSS catalogue are known to be accurate to 2 per cent, given the same caveats associated with VSAD explained in this paper (Condon et al. 1998). Figure 8 shows the distribution of spectral index (α)[3] between SUMSS and NVSS in three flux density bins. This was determined by crossmatching all sources in the SUMSS-NVSS overlap region ($-40° \le \delta \le -30°$) with position offset no greater than 30″ and only a single match within 100″. This resulted in 7643 matches. The overall median spectral index is −0.83, which is consistent with previous determinations of spectral index at frequencies below 1.4 GHz (Oort et al. 1988; Hunstead 1991; De Breuck et al. 2000). A tail of flat spectrum ($\alpha \sim 0$) sources (probably QSOs) can be seen in the top panel. The FWHM of the distributions increases from 0.7 in the upper panel to 1.2 in the lower panel reflecting the increasing uncertainty in flux density for $S_{843} < 20$ mJy. The steep and flat spectrum tails ($\alpha < -2.0$ and $\alpha > 1.0$ respectively) in the bottom panel were checked visually and found to be due to fitting errors and erroneous flux densities in both NVSS and SUMSS.

5 CATALOGUE FORMAT

Table 3 shows the format of the SUMSS catalogue. The catalogue will be available as a large text file accessible via the web. A short description of each of the columns of the catalogue follows.

Columns (1) & (2): The right ascension (α) and declination (δ) of the source in J2000 coordinates.

[3] In this paper we define spectral index α to be $S_\nu \propto \nu^\alpha$

Table 2. Measurements of Molonglo Calibrators.

Calibrator[a] Name	α (B1950)[a] *h m s*	δ (B1950)[a] ° ′ ″	S_{843} Nominal[a] (Jy)	S_{843} Measured[b] (Jy)	$\sigma_{\rm rms}$[c] per cent of Measured
0252–712	02 52 26.63	−71 16 47.3	9.21	9.13 ± 0.01	2.1
0409–752	04 09 58.45	−75 15 05.7	19.80	20.21 ± 0.03	2.4
0420–625	04 20 18.61	−62 30 40.9	5.62	5.49 ± 0.02	2.8
1814–519	18 14 07.92	−51 59 20.0	6.51	6.55 ± 0.02	3.7
1814–637	18 14 45.94	−63 47 03.1	20.22	20.04 ± 0.05	3.6
1827–360	18 27 36.86	−36 04 38.1	13.86	13.72 ± 0.06	3.6
2323–407	23 23 51.69	−40 43 48.8	5.21	5.16 ± 0.03	3.8

NOTES:
[a] The source names, positions and values of nominal flux density are taken from Campbell-Wilson & Hunstead (1994).
[b] The values of measured flux density have been corrected for effects described in Gaensler & Hunstead (2000) and are average measured values for the 12-year period.
[c] The rms in flux density measurements as a percentage of measured flux density from observations, used to define the calibration uncertainty of the MOST.

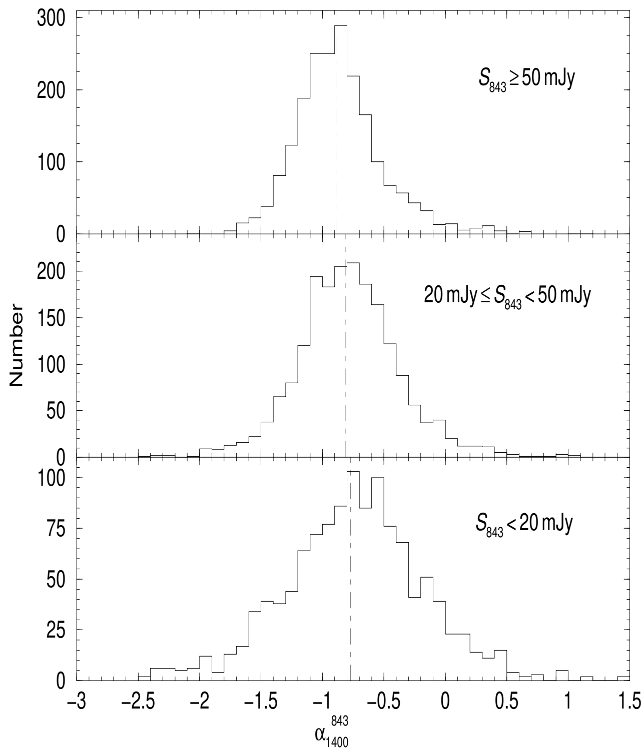

Figure 8. The spectral index distribution in the NVSS-SUMSS overlap region binned into three flux density ranges. A dotted line showing the median spectral index in each flux density bin is shown. The median spectral index increases from −0.89 at $S_{843} \geq$ 50 mJy to −0.77 at $S_{843} <$ 20 mJy. A tail of flat spectrum sources can be seen for $S_{843} \geq$ 50 mJy. The scatter in the spectral index increases with decreasing flux density.

Column (3): The uncertainty in Right Ascension in seconds of arc, calculated from the quadratic sum of the MOST Right Ascension calibration uncertainty (1.″1) and equation 2.
Column (4): The uncertainty in Declination in seconds of arc, calculated from the quadratic sum of the MOST Declination calibration uncertainty (1.″6) and equation 3.

Column (5): The peak brightness in units of mJy beam^{-1} and its associated uncertainty calculated from the quadratic sum of equation 8 and the MOST flux density calibration uncertainty of 3 per cent.
Column (6): The total flux density in units of mJy and its associated uncertainty, calculated from the equations described in C97.
Columns (7) & (8): The fitted major & minor axes of the source in arcseconds.
Column (9): The fitted major axis position angle of the source in degrees east of north. Most unresolved sources would have PA values close to 0° or 180° since the MOST elliptical beam has PA=0.
Column (10): If the fitted major axis size exceeds the beam size by more than $2.33\sigma(\theta_{\rm M})$, the major axis size after deconvolution from the MOST beam is given in arcseconds.
Column (11): If the major axis is resolved the minor axis is subsequently checked using the same criterion. If the minor axis is found to be resolved the deconvolved minor axis size is given in arcseconds.
Column (12): If the major axis is resolved, its deconvolved position angle in degrees east from north is given.
Column (13): The name of the mosaic in which the source appears. The original mosaics are available online at http://www.astrop.physics.usyd.edu.au/mosaics. In the case of duplicate matches the mosaic name quoted is that used for the fit which is chosen to be included in the catalogue.
Column (14): The number of mosaics in which the source appears. This is included to let the user know when the source appears in more than one image. The source parameters which appear in the catalogue are those for the most reliable fit.
Columns (15) & (16): The X & Y pixel positions of the source on the quoted mosaic.

Table 3. The First Page of the SUMSS Catalogue.

(1) α (J2000) $h\ m\ s$	(2) δ (J2000) $^\circ\ '\ ''$	(3) $\Delta\alpha$ $''$	(4) $\Delta\delta$ $''$	(5) $A^{\rm a}_{843}$ mJy beam^{-1}	(6) σ_A	(7) $S^{\rm b}_{843}$ mJy	(8) σ_S	(9) $\theta_{\rm M}{}^{\rm c}$ $''$	(10) $\theta_{\rm m}{}^{\rm c}$ $''$	(11) ${\rm PA_F}{}^{\rm c,d}$ $^\circ$	(12) $\phi_{\rm M}{}^{\rm e}$ $''$	(13) $\phi_{\rm m}{}^{\rm e}$ $''$	(14) ${\rm PA_S}{}^{\rm e,d}$ $^\circ$	(15) Mosaic[f]	(16) #[f]	(17) X-Pixel	(18) Y-Pixel
00 00 00.00	−31 09 52.24	4.4	4.6	12.1	1.4	13.8	1.6	84.9	58.4	41.3	0.0	0.0	---	J0000M32	1	705.0	518.9
00 00 02.31	−37 08 00.38	2.3	3.4	13.2	1.2	13.3	1.2	76.6	45.3	177.2	0.0	0.0	---	J0000M36	1	702.5	197.0
00 00 03.28	−75 01 02.93	1.8	2.1	29.4	1.5	33.0	1.7	58.6	45.0	5.4	35.8	0.0	5.9	J0000M76	1	703.8	996.0
00 00 03.29	−66 05 43.51	1.7	1.8	25.6	1.0	25.7	1.0	50.1	45.0	90.7	0.0	0.0	---	J0000M64	2	703.2	17.8
00 00 04.14	−64 19 06.06	3.5	3.9	7.4	0.9	7.4	0.9	50.1	45.1	173.1	0.0	0.0	---	J0000M64	1	702.6	540.4
00 00 04.61	−75 12 43.42	4.3	4.8	9.7	1.4	11.4	1.6	57.4	50.1	16.1	0.0	0.0	---	J0000M76	1	703.4	934.2
00 00 06.14	−29 55 10.49	4.5	7.6	11.8	2.1	13.1	2.3	93.0	51.0	169.4	0.0	0.0	---	J0000M32	1	697.7	734.7
00 00 06.39	−34 19 06.49	4.0	5.8	10.4	1.6	10.9	1.7	76.6	49.5	11.6	0.0	0.0	---	J0000M36	1	697.8	738.4
00 00 06.39	−63 11 52.08	1.8	1.8	34.0	1.3	43.8	1.7	75.9	49.5	67.2	60.6	0.0	69.9	J0000M64	1	701.1	870.0
00 00 06.43	−69 25 35.54	1.5	1.7	118.9	3.6	118.9	3.6	48.6	45.0	91.6	0.0	0.0	---	J0000M68	1	701.9	221.2
00 00 07.78	−70 21 10.15	1.9	2.1	18.2	0.9	18.2	0.9	47.3	45.3	17.9	0.0	0.0	---	J0000M72	1	701.4	1182.6
00 00 07.96	−72 36 43.24	2.2	2.3	14.2	0.9	14.5	0.9	48.0	46.0	38.7	0.0	0.0	---	J0000M72	1	701.8	479.5
00 00 08.22	−37 38 19.61	3.1	3.3	18.1	1.5	20.8	1.7	76.6	59.9	41.6	0.0	0.0	---	J0000M36	1	696.1	99.8
00 00 08.89	−71 00 19.76	2.3	2.5	13.2	0.9	13.3	0.9	47.3	45.6	151.2	0.0	0.0	---	J0000M72	1	701.1	979.5
00 00 09.90	−31 33 30.53	1.6	2.1	44.7	2.0	44.7	2.0	84.9	45.1	0.9	0.0	0.0	---	J0000M32	1	693.5	450.6
00 00 10.70	−63 04 14.09	2.8	2.9	11.3	1.0	13.0	1.1	62.4	47.6	42.1	0.0	0.0	---	J0000M64	1	698.4	907.4
00 00 10.86	−72 12 53.71	1.7	1.9	25.0	1.1	25.2	1.1	47.3	45.5	119.1	0.0	0.0	---	J0000M72	1	700.5	603.1
00 00 11.43	−85 39 20.09	1.5	1.7	101.6	3.1	102.9	3.2	46.3	45.2	65.9	0.0	0.0	---	J0000M84	3	703.8	162.2
00 00 11.82	−82 47 32.39	1.7	1.8	74.4	2.7	101.0	3.7	69.0	54.4	66.9	52.3	30.2	67.2	J0000M84	1	703.0	1094.0
00 00 11.93	−66 30 45.94	1.5	1.7	93.5	2.9	98.2	3.1	53.0	45.4	5.7	21.4	0.0	10.1	J0000M68	1	698.5	1105.2
00 00 13.15	−63 34 57.29	3.6	3.5	10.3	1.0	13.4	1.4	79.8	48.2	48.8	0.0	0.0	---	J0000M64	1	697.0	756.8
00 00 13.17	−72 59 54.71	1.8	1.9	28.1	1.2	29.9	1.3	51.2	47.2	103.6	0.0	0.0	---	J0000M72	1	699.7	359.2
00 00 13.29	−35 55 20.96	3.8	3.1	12.2	1.3	12.6	1.3	76.6	48.3	63.2	0.0	0.0	---	J0000M36	1	690.3	429.9
00 00 14.02	−34 10 00.23	1.7	2.0	65.4	2.5	77.0	3.0	76.6	62.4	150.2	0.0	0.0	---	J0000M36	1	689.2	767.6
00 00 15.68	−76 56 30.59	1.5	1.7	84.5	2.7	86.3	2.8	48.3	45.1	11.9	0.0	0.0	---	J0000M76	1	700.2	384.9
00 00 15.77	−33 12 21.60	3.2	2.3	17.0	1.4	17.1	1.4	84.9	45.7	78.0	0.0	0.0	---	J0000M32	1	687.0	164.9
00 00 15.86	−70 49 28.88	2.8	3.2	10.0	1.0	10.5	1.0	52.0	45.2	14.1	0.0	0.0	---	J0000M72	1	697.9	1035.8
00 00 17.30	−82 40 59.16	2.2	2.3	23.8	1.5	23.8	1.5	45.2	45.0	65.8	0.0	0.0	---	J0000M84	1	702.0	1129.6
00 00 17.37	−37 28 25.07	2.8	4.2	11.2	1.3	11.3	1.3	76.6	45.7	4.3	0.0	0.0	---	J0000M36	1	686.2	131.6
00 00 17.76	−34 10 40.26	1.6	1.7	126.4	4.1	132.4	4.3	76.6	49.4	116.7	0.0	0.0	---	J0000M36	1	685.0	765.5
00 00 17.84	−35 18 07.16	4.0	3.7	14.5	1.5	16.3	1.7	76.6	57.1	122.0	0.0	0.0	---	J0000M36	1	685.1	549.3
00 00 17.94	−37 21 00.68	3.0	3.5	16.7	1.4	19.3	1.6	76.6	59.9	154.1	0.0	0.0	---	J0000M36	1	685.6	155.3

NOTES:
[a] The peak brightness of the gaussian fit in units of mJy beam^{-1}. This value may be in error by more than the quoted error for extended sources.
[b] The total flux density of the gaussian fit in units of mJy. $S = A$ for point sources.
[c] The widths and position angle of the fitted gaussian. The fit is constrained so that $\theta_{\rm m} \geq 45''$ (the beam minor axis width).
[d] The position angle of the major axis is measured in degrees East from North.
[e] The deconvolved widths and position angle of the source. A value is given only if the fitted axis exceeds the beam by more than $2.33\sigma_\theta$
[f] The name of the mosaic the quoted source can be found in. If the number in the next column is greater than 1 it can also be found in neighbouring mosaics.

Please refer to SUMSS catalogue sources by their full IAU designations (Lortet et al. 1994). These are of the form SUMSS *JHHMMSS−DDMMSS* where SUMSS is the survey acronym, *J* specifies J2000.0 coordinate equinox, *HHMMSS* are the hours, minutes and truncated seconds of right ascension, − is the sign of declination and *DDMMSS* are the degrees, minutes and truncated seconds of declination. For example the SUMSS source in Table 3 at J2000.0 coordinates $\alpha = 00^h00^m08\overset{s}{.}89$, $\delta = -71°00'19\overset{''}{.}76$ is called SUMSS J000008−710019.

6 ANALYSIS

The following section contains results of our analysis of the catalogue. Our goal in producing the SUMSS catalogue has been to create a source list which is as reliable as possible. This implies that all the sources which appear should be genuine. In this section we also examine the uniformity of the catalogue. An adequate determination of 843 MHz source counts and the two-point angular correlation function will require a catalogue with uniform source density (Blake & Wall 2002). Finally the SUMSS catalogue is compared with catalogues at other frequencies as an independent check of the accuracy of quoted source characteristics.

6.1 Reliability and Completeness

The rms noise level in SUMSS mosaics is not uniform across the survey. It can increase substantially close to bright sources and changes strongly with declination (see Figure 4). In surveys with uniform noise levels a 5σ limiting amplitude is applied to catalogues made from them (Murdoch et al. 1973). As the noise is not uniform in SUMSS the limiting peak amplitude varies from 4σ to 6σ depending on the position of each source in the survey.

To estimate how the SUMSS catalogue reliability varies with amplitude we have searched 5 northern mosaics to 2σ and crossmatched all fitted sources with the NVSS. The NVSS is believed to be better than 90 per cent reliable at flux densities above 5 mJy at 1.4 GHz (Condon et al. 1998) and so should be a good independent check of the reliability of SUMSS. We define the reliability at amplitude A_{843} as the number of SUMSS sources with an NVSS counterpart within 50″ divided by the total number of SUMSS sources. There is about a 3 per cent chance of an NVSS position being within 50″ of a random SUMSS noise peak.

Figure 9 shows a plot of the reliability of SUMSS as a function of peak flux density. At the 4σ level, the catalogue is still around 80 per cent reliable and this increases to 90 per cent at around 4.5σ. The SUMSS catalogue is therefore still reliable below 5σ, predominantly because the decision tree is trained to remove spurious responses.

Fitting errors and confusion in the MOST beam can affect the completeness of the catalogue at fainter flux densities. The decision tree is geared towards removing poorly fitted sources at lower flux density and this may also affect the completeness. We have attempted to determine the completeness of the SUMSS catalogue by running simulations. We placed 1000 artificial point sources of varying flux density into a selection of mosaics and performed the normal cataloguing procedures on them.

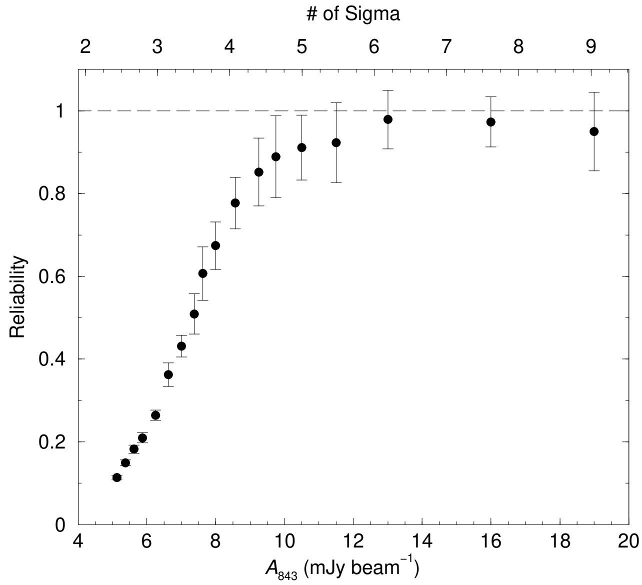

Figure 9. The fraction of SUMSS sources detected in the NVSS catalogue vs. peak flux density. At the catalogue limit of 10 mJy beam^{-1} about 90 per cent of SUMSS sources are detected in NVSS. Sigma has been calculated as the median local rms noise of all sources in this plot (1σ=2.1 mJy beam^{-1}). At these flux densities the NVSS is also about 90 per cent reliable.

Figure 10 shows the fraction of artificial point sources which were catalogued vs. flux density. In fitting the 1000 point sources no particular biases were evident. The shape of the distributions is quite different for northern and southern mosaics. For southern mosaics the plot shows that the SUMSS catalogue is ∼ 60 per cent complete at the limiting flux density of 6 mJy and this increases to 100 per cent at 8 mJy. For northern mosaics the catalogue is ∼ 40 per cent complete at 10 mJy and 100 per cent complete at 18 mJy. The more extended distribution in the northern catalogue is because the mosaics here are noisier and the beam is larger, resulting in greater confusion. The decision tree has had no significant detrimental effect on the completeness for point sources. This is because artefacts generally mimic extended sources and the decision tree tends to remove extended sources at lower flux density rather than point sources.

6.2 Source Density

Table 4 of Paper I (Bock et al. 1999) shows integral source counts at 843MHz taken from Large (1990) and we are now able to compare the source counts in that table with those derived in the SUMSS survey. The source density has been determined from a selection of non-overlapping mosaics in the catalogue and the results of this analysis are shown in Figure 11. To examine the effect of the decision tree on the source density, we have plotted the source density both before and after its application. The source density derived from the raw catalogue will contain artefacts as well as real sources while the classified catalogue should only have real sources, although some real sources may have been erroneously removed by the decision tree.

For $S_{843} \geq 6$ mJy Large (1990) estimated an 843 MHz

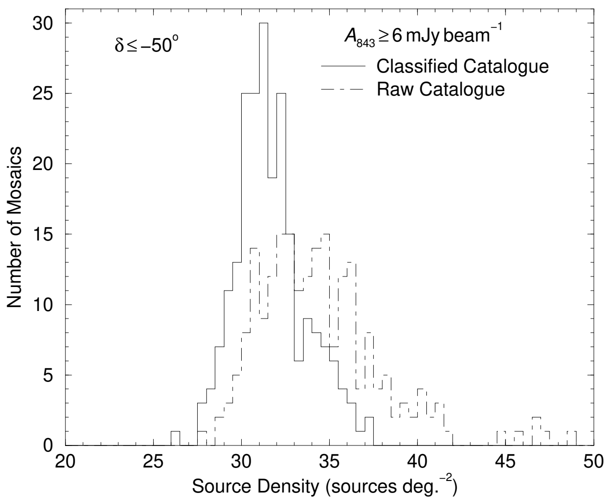

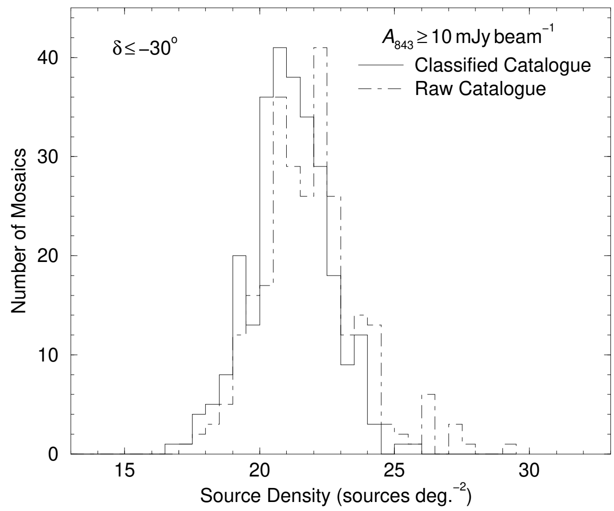

Figure 11. Histograms showing the source density of the SUMSS catalogue before and after the application of the decision tree. The source density was calculated for each mosaic and a random selection of non-overlapping mosaics was chosen so as to keep the data independent. The plot on the left is for southern sources with $A_{843} \geq 6\,\mathrm{mJy\,beam^{-1}}$. Northern and southern sources are grouped in the plot on the right, which shows the source density for sources with $A_{843} \geq 10\,\mathrm{mJy\,beam^{-1}}$.

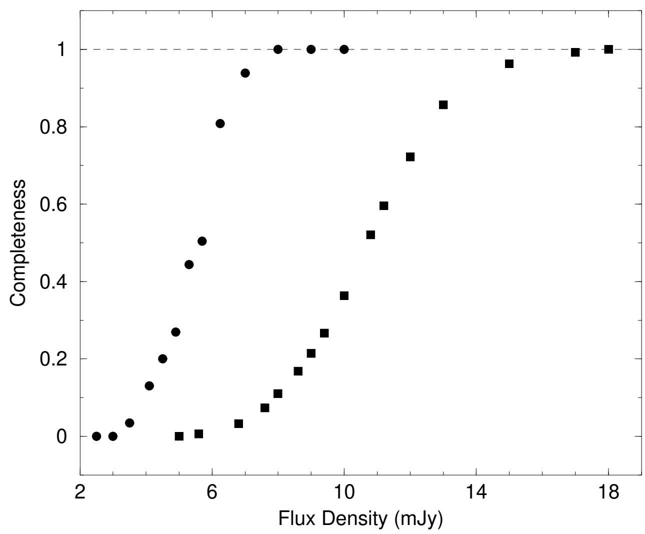

Figure 10. The fraction of artificial point sources which are catalogued vs. Flux Density. The circles are for southern mosaics ($\delta \leq -50°$) and the squares are for northern ones ($\delta > -50°$). A dashed line at 100 per cent is shown. At 6mJy (the limit of the southern catalogue) the completeness for southern mosaics is around 60 per cent and this rises rapidly to 100 per cent at 8 mJy. At 10 mJy the completeness for the northern catalogue is about 40 per cent. The northern catalogue is 100 per cent complete above about 18 mJy.

source density of 31 ± 3 sources deg^{-2}. Figure 11 (left) shows the source density in southern mosaics limited to peak brightness $A_{843} \geq 6\,\mathrm{mJy\,beam^{-1}}$. The distribution before application of the decision tree has an average of 36.3 ± 0.6 sources deg^{-2} and, after classification, 31.6 ± 0.1 deg^{-2}. Outliers in the distribution are attributed to mosaics with strong sources which produce many artefacts. In the raw catalogue these artefacts are fitted as sources, producing an increased source density for that mosaic. In the classified catalogue, the source density is not uniform because the local rms noise close to strong sources is higher than in other regions.

The effect of the decision tree is less pronounced at $A_{843} \geq 10\,\mathrm{mJy\,beam^{-1}}$. Large (1990) determined a source density of $21 \pm 2\,\mathrm{deg^{-2}}$. The plot on the right in Figure 11 shows the distribution of source densities in the same set of southern mosaics with the addition of non-overlapping northern mosaics with $A_{843} \geq 10\,\mathrm{mJy\,beam^{-1}}$. For $A_{843} \geq 10\,\mathrm{mJy\,beam^{-1}}$ the distribution is very similar for both the raw and classified catalogues and indicates that our decision tree is predominantly affecting sources of peak brightness less than $10\,\mathrm{mJy\,beam^{-1}}$ (see Figure 15). The average source density for the raw catalogue is $22.1 \pm 0.2\,\mathrm{deg^{-2}}$ and the average for the classified catalogue is $21.1 \pm 0.1\,\mathrm{deg^{-2}}$.

Our results are in good agreement with those derived by Large (1990) from a much smaller survey area. One important aspect of the distribution of source density in the classified catalogue is that there is less scatter between mosaics after the application of the decision tree. This indicates that the decision tree is making the catalogue more uniform.

Figure 12 shows the variation of source density in the catalogue with declination. This has been determined for three different flux density cutoffs ($A_{843} \geq 6\,\mathrm{mJy\,beam^{-1}}$, $A_{843} \geq 10\,\mathrm{mJy\,beam^{-1}}$ & $S_{843} \geq 20\,\mathrm{mJy}$). The lines in the plot are the values of source density from Large (1990) for the three flux density cutoffs. We expect the SUMSS catalogue to be 100 per cent complete above 20 mJy so we directly compare the counts for integrated flux density with those quoted by Large (1990). We believe the source counts quoted by Large (1990) may have been underestimated due to the small area of sky used (about 28 deg^2).

Figure 12 is similar to that made for the NVSS survey by Blake & Wall (2002) but does not show the same scatter evident in their results. Blake & Wall (2002) attributed their results to the change from the DnC to the D configuration of the VLA for the NVSS survey at different declinations. No such change takes place on the MOST, thereby resulting in

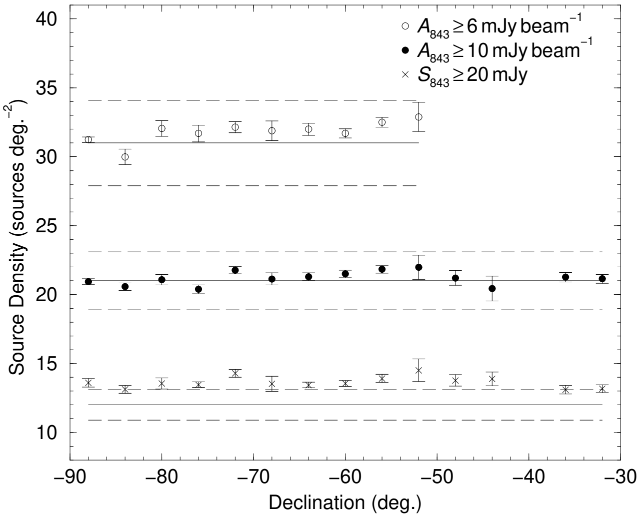

Figure 12. The variation in source density with declination for different flux density limits shows little scatter across the survey. This is primarily because the telescope does not change its configuration at different declinations. The lines are the values of source count values from Large (1990) with their associated 10 per cent uncertainty. A peak brightness cutoff was applied at both 10 and 6 mJy beam^{-1} and a total flux density cutoff was applied at 20 mJy, where we expect the catalogue to be complete.

Table 4. MRC sources missing from the SUMSS catalogue

MRC Name	α (J2000) h m s	δ (J2000) $°$ $'$ $''$	S_{408} Jy
MRC B0536−692[1]	05 36 20.7	−69 12 15	1.03
MRC B0540−697[1]	05 39 58.5	−69 45 00	2.22
MRC B1737−602	17 42 02.9	−60 15 54	0.80
MRC B1754−577[2]	17 59 05.2	−57 42 20	1.21
MRC B1817−632[2]	18 22 16.0	−63 10 41	0.90
MRC B2220−700	22 24 39.6	−69 47 42	0.73

NOTES:
[1] H II regions located in the LMC.
[2] Spurious north-south sidelobes of the Mills Cross.

a survey which is more uniform with declination, especially at flux densities greater than 10mJy.

6.3 SUMSS–MRC Crossmatch

As a separate check of the catalogue completeness for brighter sources, the SUMSS catalogue was cross-matched with the Molonglo Reference Catalogue (MRC; Large et al. 1981, 1991). The MRC was made from $2\farcm62 \times 2\farcm86 \sec(\delta + 35\fdg5)$ resolution observations at 408 MHz using the Mills Cross Radio Telescope (Mills et al. 1963), the previous incarnation of the MOST. The MRC is complete to $S_{408} = 1$ Jy at 408 MHz and has a (non-uniform) limiting flux density of $S_{408} = 0.7$ Jy. Given a spectral index of $\alpha = -0.8$ we expect the faintest MRC sources to appear in the SUMSS catalogue at around $S_{843} = 400$ mJy and certainly no fainter than $S_{843} = 150$ mJy. This implies that all MRC sources should appear in the SUMSS catalogue.

There are 1670 MRC sources in the area covered by the SUMSS catalogue. Of these only 46 were found not to have a match within 60″ in SUMSS. Upon closer inspection it was revealed that many of these initial non-detections were actually sources which were resolved into doubles in SUMSS; for these sources there are two entries in the SUMSS catalogue around 100″ from the single source in the MRC. Of the sources which are detected, we determine a median spectral index between 408 MHz and 843 MHz of $\alpha = -0.95$.

Two of the missing MRC sources (Centaurus A & NGC 5090) were found to be fitted quite badly by VSAD. Fits to these sources were modified. They have not been assigned a peak amplitude or source size, only a position and total flux density. The total flux density of these sources has been determined by summing the pixels inside a hand defined source area using the CGCURS routine in MIRIAD. We may add other complex sources by hand in future releases of the catalogue.

The MRC sources not detected in SUMSS are tabulated in Table 4. Some of the sources are H II regions in the Large Magellanic Cloud which, although point sources in the MRC, appear quite complex in the smaller MOST beam. Elliptical gaussians fitted to these sources were automatically removed by the decision tree and have been left out of the catalogue.

The four sources away from the Clouds are particularly interesting. The positions of these sources have been inspected in the original SUMSS images and are not detected at even a 3σ limit. Two of the sources, MRC B1817–632 and MRC B1754–577 were observed with the Australia Telescope Compact Array at 1.4 GHz and no source was detected to a 3σ limit of 0.5 mJy at both MRC positions. All of the original 408 MHz data obtained with the Mills Cross telescope are currently being reprocessed by D. Crawford (private communication) and from this reprocessing a new deeper 408 MHz catalogue is being produced. Examination of the reprocessed data has revealed that both MRC B1817−632 and MRC B1754−577 appear to be anomalous north-south sidelobes. However, the other two sources (MRC B1737−602 and MRC B2220−700) appear to be genuine in the 408 MHz catalogue. A $b_J = 16.75$ magnitude galaxy is located at the position of MRC B2220−700. It is difficult to know at this stage if MRC B1737−602 and MRC B2220−700 are transient phenomena or form part of a population of objects whose spectra peak at very low frequency.

6.4 Resolved Sources

In the current release of the SUMSS catalogue about 10 per cent of sources are found to be resolved. This fraction varies from 25 per cent at $\delta = -88°$ to 2 per cent at $\delta = -32°$ where the beam area is almost doubled. Almost all resolved sources are extended in only one direction; only 1 per cent of sources are resolved in both axes.

To check the accuracy of deconvolved source sizes in the SUMSS catalogue, sizes and position angles of resolved sources were compared with the sizes of resolved sources in the NVSS catalogue. Almost all sources found to be resolved in SUMSS were also resolved in the NVSS; the small fraction that were not were attributed to the effects described below.

A comparison of the source widths in SUMSS and NVSS is shown in Figure 13. For about half of the sources the ma-

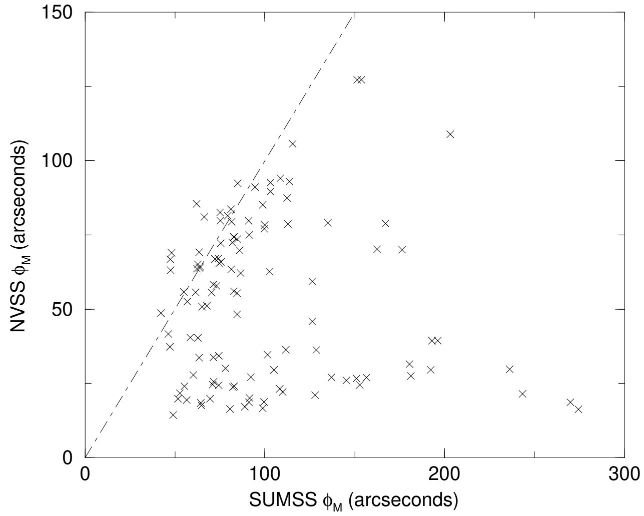

Figure 13. The distribution of major axis lengths in SUMSS and NVSS. There is a class of SUMSS sources with large angular sizes which appear to be barely resolved in NVSS. This is due to a mixture of fitting problems in VSAD and the increased surface brightness sensitivity of the MOST. A small number of sources which are fitted as one elongated gaussian in SUMSS are fitted as two separate unresolved components in the NVSS, this is because of the larger MOST beam.

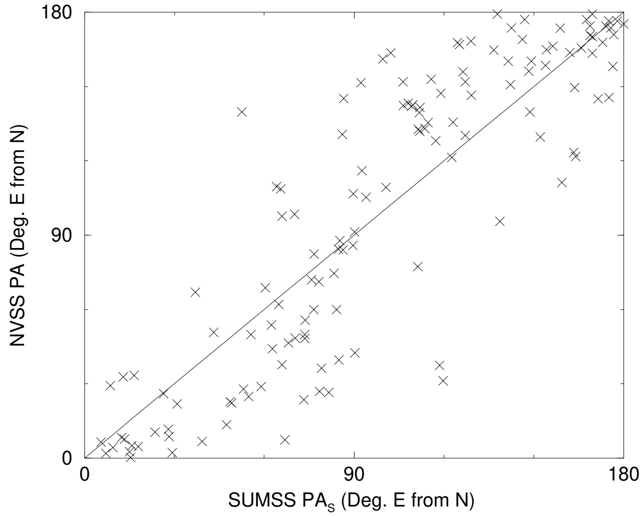

Figure 14. The distribution of position angles of resolved sources in SUMSS and NVSS. There is a general agreement in position angle between the two surveys. Sources with position angles close to 0° in one survey can sometimes be found close to 180° in the other, this explains the outlying points found on the top left and bottom right corners of the plot.

jor axis widths agree well between the two surveys. However, there is a substantial group of sources which has a larger major axis in SUMSS. Many of these sources seem to be fitted accurately by VSAD and probably form a class of objects in which much of their structure has been resolved out in the NVSS images, but is preserved in the SUMSS survey. This is because of the continuous UV coverage of the MOST (Bock et al. 1999). Visual inspection of other sources reveals some of them are poorly fitted by the VSAD program, as illustrated in Figure 2. These sources are all genuinely resolved close doubles but VSAD has fitted a gaussian of major axis much longer than the source. Figure 14 shows the distribution of position angles between sources in the two surveys, these are generally in reasonable agreement given the very different raw beamshapes in the two surveys.

6.5 Source Counts

Figure 15 shows the differential source counts in the southern part of the SUMSS catalogue normalised to a euclidean universe. The source counts shown here are plotted using peak amplitudes and are used to show the effectiveness of the decision tree. The true source counts at 843 MHz should resemble those shown here fairly closely as only 10 per cent of sources in the catalogue are resolved. Also, no account is made here for the decrease in source density close to brighter sources. A more thorough source count determination will follow in a later paper.

The effect of the decision tree is quite pronounced in this plot. Artefacts cause the source counts to tail upwards below about 10 mJy beam^{-1}. The decision tree is affecting the counts below this level, causing the counts to flatten to the same slope as that above 10 mJy beam^{-1}. This suggests that the decision tree is doing an excellent job of removing artefacts. Users should note that the decision tree is having its greatest effect below 10 mJy beam^{-1}, so above this level the catalogue is mostly unaltered from its raw state.

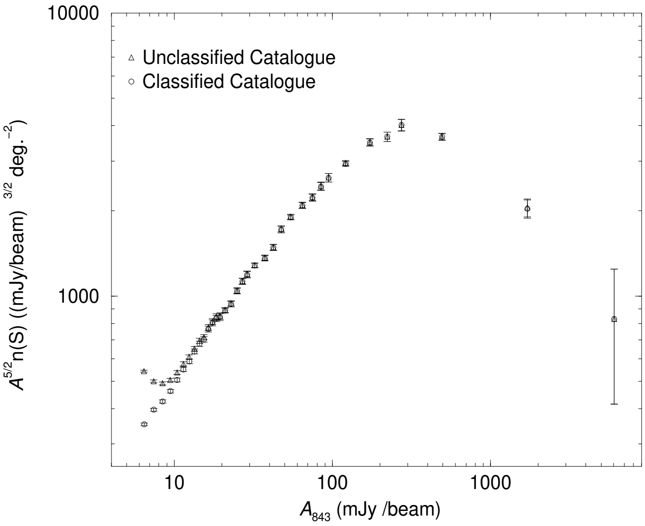

Figure 15. The normalised source counts derived from peak amplitude for the southern part of the catalogue. As most sources in the survey are unresolved this determination should closely resemble the counts for total flux density. The counts in the catalogue before and after application of the decision tree are presented. Artefacts are affecting the decision tree at flux density levels below 10 mJy beam^{-1} and the decision tree is restoring the counts to the slope which is expected in this region.

7 SUMMARY

We have created a catalogue of 107,765 sources over the 3500 deg^2 of the SUMSS survey currently available. It is expected the survey will be complete by the end of 2003. Until then we will endeavour to update the catalogue as new mosaics are released. The survey is currently progressing at the rate of 1500 $\deg^2$ per year and we expect the coverage of the catalogue to increase at a similar rate. As coverage gaps in the survey are filled positions and flux densities at the edges of currently released regions may change due to the increased sensitivity from overlapping fields. We will maintain backups of each release of the catalogue so that users may continue to have access to versions of the catalogue they may previously have used.

We believe the southern catalogue to be 100 per cent complete above ∼8 mJy and the northern catalogue to be complete above ∼18 mJy. Below these flux densities, confusion and the decision tree have affected the completeness, but we expect the catalogue to be highly reliable. The catalogue has a source density of 32 $\deg^{-2}$ above 6 mJy beam^{-1} and 21 $\deg^{-2}$ above 10 mJy beam^{-1}. Users should note that some sources (especially those which are resolved) may have positions and flux densities outside the quoted uncertainties. Users are encouraged to check the $4.3^\circ \times 4.3^\circ$ mosaics if in doubt.

The catalogue is publicly available and the current version as well as future updates can be found at www.astrop.physics.usyd.edu.au/sumsscat/.

ACKNOWLEDGMENTS

The Molonglo Observatory site manager, Duncan Campbell-Wilson, and the staff, Jeff Webb, Michael White and John Barry are responsible for the smooth operation of the MOST telescope and the day to day observing program of the SUMSS survey. For this we give them heartfelt thanks. Bruce McAdam and Tony Turtle provided valuable information on artefacts in MOST images and deconvolution. Tony Turtle is also responsible for SUMSS scheduling. The SUMSS survey is dedicated to Michael Large whose expertise and vision made the project possible. We would also like to thank the referee J. Condon for some useful suggestions. The MOST is operated with the support of the Australian Research Council and the Science Foundation for Physics within the University of Sydney.

REFERENCES

Beichman C. A., Neugebauer G., Habing H. J., Clegg P. E., Chester T. J., 1988, Infrared astronomical satellite (IRAS) catalogs and atlases. Volume 1: Explanatory supplement, Vol. 1. NASA RP–1190, Washington, DC:GPO

Blake C., Wall J., 2002, MNRAS, 329, L37

Bock D. C.-J., Large M. I., Sadler E. M., 1999, ApJ, 117, 1578

Campbell-Wilson D., Hunstead R. W., 1994, PASA, 11, 33

Condon J. J., 1997, PASP, 109, 166

Condon J. J., Cotton W. D., Greisen E. W., Yin Q. F., Perley R. A., Taylor G. B., Broderick J. J., 1998, AJ, 115, 1693

De Breuck C., van Breugel W., Röttgering H. J. A., Miley G., 2000, A&AS, 143, 303

Gaensler B. M., Hunstead R. W., 2000, PASA, 17, 72

Green A. J., 1999, in ASP Conf. Ser. 168: New Perspectives on the Interstellar Medium, p. 43

Green A. J., Bunton J. D., Campbell-Wilson D., Cram L. E., Davison R. G., Hunstead R. W., Mitchell D. A., Parfitt A. J., 2001, in SKA: Defining the Future, Berkeley, U.S.A., www.skatelescope.org/skaberkely/

Hunstead R. W., 1991, Australian Journal of Physics, 44, 743

Large M. I., Campbell-Wilson D., Cram L. E., Davison R. G., Robertson J. G., 1994, PASA, 11, 44

Large M. I., Cram L. E., Burgess A. M., 1991, The Observatory, 111, 72

Large M. I., Mills B. Y., Little A. G., Crawford D. F., Sutton J. M., 1981, MNRAS, 194, 693

Lortet M.-C., Borde S., Ochsenbein F., 1994, A&AS, 107, 193

Mills B. Y., 1981, PASA, 4, 156

Mills B. Y., Aitchison R. E., Little A. G., McAdam W. B., 1963, Proc. Inst. Radio Engrs Aust., 24, 156

Murdoch H. S., Crawford D. F., Jauncey D. L., 1973, ApJ, 183, 1

Oort M. J. A., Steemers W. J. G., Windhorst R. A., 1988, AAS, 73, 103

Quinlan J., 1993, C4.5: Programs for Machine Learning. Morgan Kaufmann, San Mateo, CA USA

Robertson J. G., 1991, Australian Journal of Physics, 44, 729

Sault R. J., Teuben P. J., Wright M. C. H., 1995, in ASP Conf. Ser. 77: Astronomical Data Analysis Software and Systems IV, Vol. 4, p. 433

Voges W., 1992, in Environment Observation and Climate Modelling Through International Space Projects, pp. 9–19

White R. L., Becker R. H., Helfand D. J., Gregg M. D., 1997, ApJ, 475, 479

Wild J. P., 1970, Australian Journal of Physics, 23, 113

Windhorst R., Mathis D., Neuschaefer L., 1990, in ASP Conf. Ser. 10: Evolution of the Universe of Galaxies, pp. 389–403